Original Research

Manipulating Histone Acetylation Leads to Antitumor Effects in Hemangiosarcoma Cells

Tamami Suzuki [1], Keisuke Aoshima [1]*, Jumpei Yamazaki [2], Atsushi Kobayashi [1], Takashi Kimura [1]

[1] *Laboratory of Comparative Pathology, Department of Clinical Sciences, Faculty of Veterinary Medicine, Hokkaido University, Sapporo, Hokkaido, 060-0818, Japan*

[2] *Translational Research Unit, Veterinary Teaching Hospital, Faculty of Veterinary Medicine, Hokkaido University, Sapporo, Hokkaido, 060-0818, Japan*

Running title: Histone Acetylation in Hemangiosarcoma

* Corresponding author. Tel.: +81 11 7065193.

E-mail address: k-aoshima@vetmed.hokudai.ac.jp (Keisuke Aoshima).

Acknowledgements

We would like to extend our sincerest gratitude to Dr. Hiroki Sakai, Gifu University, for providing canine hemangiosarcoma cell lines. We also acknowledge the efforts of Drs. Mitsuyoshi Takiguchi, Shintaro Kobayashi, and Hironobu Yasui, Faculty of Veterinary Medicine, Hokkaido University for giving useful pieces of advice and constructive discussion. We are grateful to all the members of the Laboratory of Comparative Pathology, Faculty of Veterinary Medicine, Hokkaido University for their helpful discussions,

encouragement, and support. This research was supported by KAKENHI Grant-in-Aid for Young Scientists (KA, Number 20K15654) provided by Japan Society for the Promotion of Science. We thank H. Nikki March, PhD, from Edanz (https://jp.edanz.com/ac) for editing a draft of this manuscript.

Conflict of interest statement

The authors declare that there is no conflict of interest in this study.

Ethics statement

The owners were thoroughly informed about the research aims and protocols, and a written consent form was obtained prior to the investigation. All mouse experiments were performed under the guidelines of Hokkaido University (protocol number: 20-0083), which follows the ARRIVE guidelines.

Preprint

The preprint of this manuscript was uploaded on bioRxiv.
https://www.biorxiv.org/content/10.1101/2021.12.10.472173v2

Data availability

The datasets generated and/or analyzed during the current study are available from the corresponding author on reasonable request.
RNA-seq data was uploaded on Gene Expression Omnibus (GEO accession GSE200106). This will be published when this manuscript is accepted. To review GEO accession GSE200106, please visit https://www.ncbi.nlm.nih.gov/geo/query/acc.cgi?acc=GSE200106.

Original Research

Title

Manipulating Histone Acetylation Leads to Antitumor Effects in Hemangiosarcoma Cells

Word count: 4000 words

Number of figures: 6

Number of Tables: 0

Abstract

Canine hemangiosarcoma (HSA) is a malignant tumor derived from endothelial cells. No effective treatment has yet been developed because of the lack of understanding of its pathogenesis. Histone acetylation, an epigenetic modification, is highly associated with cancer pathogenesis. Manipulating histone acetylation by histone deacetylase inhibitors (HDACi) or bromodomain and extraterminal domain inhibitors (BETi) is one approach to treat various cancers. However, the role of histone acetylation in HSA remains unknown. This study aimed to investigate how histone acetylation functions in HSA pathogenesis using two HDACi, suberanilohydroxamic acid (SAHA) and valproic acid (VPA), and one BETi, JQ1, *in vitro* and *in vivo*. Histone acetylation levels were high in cell lines and heterogeneous in clinical cases. SAHA and JQ1 induced apoptosis in HSA cell lines. HSA cell lines treated with SAHA and VPA upregulated inflammatory-related genes and attracted macrophage cell line RAW264 cells, which suggests that SAHA and VPA can affect immune responses. JQ1 stimulated autophagy and inhibited the cell cycle in HSA cell lines. Finally, we demonstrated that JQ1 suppressed HSA tumor cell proliferation *in vivo* although SAHA and VPA did not affect tumor growth. These results suggest that BETi can be alternative drugs for HSA treatment. Although further research is required, our study indicated that dysregulation of histone acetylation is likely to be involved in HSA malignancy.

Keywords

BETi; HDACi; hemangiosarcoma; histone acetylation

31 **1. INTRODUCTION**

32 Canine hemangiosarcoma (HSA) is a malignant tumor derived from endothelial cells.
33 It is characterized by invasive growth and high metastatic rates, which causes high mortality
34 to patients.[1] Surgery and chemotherapy are conventional therapies for HSA, but the efficacy
35 of these treatments was limited.[2] Angiosarcoma (AS), a counterpart of HSA in humans, has
36 similar clinicopathological features to HSA.[3,4] Somatic mutations in *PIK3CA*, *TP53* or *RASA1*
37 were identified in both HSA and AS,[5] but little is known about how these mutations relate to
38 HSA and AS pathogenesis.

39 Epigenetics such as DNA methylation and histone modifications regulates
40 transcription, and it is involved in various biological processes such as embryonic
41 development, metabolism, and diseases including cancer.[6–8] Acetylated histone can promote
42 transcription by binding to bromodomain and extraterminal (BET) proteins and loosening the
43 chromatin structure by neutralizing the electric charges.[9,10] In recent years, a growing number
44 of reports have highlighted that altered histone acetylation is involved in cancer
45 pathogenesis.[11,12] Histone deacetylase inhibitors (HDACi) and BET inhibitors (BETi) have
46 been used to investigate the function of histone acetylation and their treatment efficacy.
47 HDACi increased histone acetylation levels by inhibiting histone deacetylase function.[13]
48 BETi binds to the functional domain of BET proteins through which BET proteins cannot
49 recognize acetylated histones.[14] Suberanilohydroxamic acid (SAHA) and valproic acid (VPA)
50 are HDACis that have been reported to induce apoptosis *in vitro* and suppress tumor
51 proliferation *in vivo* in human cancers.[15–18] SAHA and VPA can also improve tumor
52 immunity, and combination therapies with immune checkpoint inhibitors or
53 chemotherapeutics enhance their efficacy in human cancers.[19–21] BETi has also been broadly
54 investigated as cancer drugs, including JQ1, which causes apoptosis, cell cycle arrest, and
55 autophagy *in vitro*, and impede tumor growth *in vivo*.[22–24] Regarding epigenetics in HSA,

56 KDM2B—a histone demethylase—has recently been found to promote tumor viability.[25]
57 However, the role of histone acetylation in HSA remains unknown.
58 Immune cells in tumor tissues play important roles in tumor progression as major
59 components of the tumor microenvironment. Some immune cells such as natural killer cells,
60 cytotoxic T cells, and M1-polarized macrophages attack tumor cells and inhibit tumor growth,
61 whereas other cells such as regulatory T cells and M2-polarized macrophages promote tumor
62 growth by secreting protumor cytokines or suppressing immune responses against tumor
63 cells.[26,27] Given that tumor cells dynamically interact with immune cells in tumor tissues,
64 investigating tumor pathogenesis in immunocompetent environments is crucial to develop
65 new therapeutics such as immunotherapy and metabolic therapy.[28–30] A mouse-derived AS
66 cell line ISOS-1, which is transplantable in BALB/c mice, has recently been revealed to have
67 similar morphological and molecular characteristics to canine HSA cell lines.[31,32] Identifying
68 pathological similarities between canine HSA cell-derived tumors and murine AS cell-derived
69 tumors in mice would be beneficial to find novel therapeutics involving the host immune
70 system by promoting syngeneic mouse model studies in HSA.
71 In this study, we aimed to investigate the role of histone acetylation and the effects of
72 HDACi and BETi on HSA. We used canine HSA cell lines and ISOS-1, a mouse AS cell line,
73 to explore whether they have similar responses to HDACi and BETi treatments and to
74 research their effects in both immunodeficient and immunocompetent environments.
75
76
77 **2. MATERIALS AND METHODS**
78 Full materials and methods are available in the supporting information.
79
80 **2.1 Histopathology and immunohistochemistry (IHC)**

81 Tumor samples were obtained from patients presenting to a veterinary hospital with
82 written informed consent (Table S1). The samples were stained with hematoxylin and eosin
83 staining. For IHC, antigens were retrieved in Tris-EDTA buffer (pH 9.0). Tissues were
84 stained with anti-acetylated histone H3 antibody (1:250; #39140, Active Motif, CA, USA)
85 overnight at 4°C and biotinylated goat anti-rabbit IgG (#426012, Nichirei biosciences) for 30
86 min at RT. The stained slides were scanned with NanoZoomer 2.0-RS (Hamamatsu
87 Photonics, Hamamatsu, Japan) and analyzed with QuPath ver.0.2.1.[33]

88

89 **2.2 Cell culture**

90 Canine aortic endothelial cells (CnAOEC: #Cn304-05, Cell Applications, CA, USA),
91 seven canine HSA cell lines (JuA1, JuB2, JuB4, Re12, Re21, Ud2, and Ud6),[34] ISOS-1
92 obtained from the Cell Resource Center for Biomedical Research Cell Bank (Tohoku
93 University),[35] and RAW264 obtained from RIKEN Bioresource Center, were cultured with
94 Dulbecco's Modified Eagle Medium (DMEM; #044-29765, Fujifilm Wako Pure Chemical
95 Industries, Osaka, Japan) supplemented with 10% fetal bovine serum (FBS; #S1580-500,
96 Biowest, UT, USA) and penicillin–streptomycin (#168-23191, Fujifilm Wako) at 37°C with
97 5% CO_2.

98

99 **2.3 Drug preparation**

100 SAHA (#10009929, Cayman Chemical, MI, USA) was dissolved in dimethyl
101 sulfoxide (DMSO) to a stock solution of 150 mg/ml. For *in vivo* studies, the stock solution
102 was diluted with 30% polyethylene glycol 400 and 5% Tween 80. VPA (#227-01071,
103 Fujifilm Wako) was dissolved in PBS. JQ1 (#T117580, Toronto Research Chemicals,

104 Toronto, Canada) was initially dissolved in DMSO to a stock solution of 50 mg/ml. For *in*
105 *vivo* studies, the stock solution was diluted with 5% Tween 80. Bafilomycin A1 (#554-29211,
106 Fujifilm Wako) was dissolved in DMSO to a stock solution of 1 mM.

107

108 **2.4 Cell viability assay**

109 Two thousand cells were treated with DMSO or five different concentrations of
110 SAHA or JQ1. Survival rates were analyzed using Cell Counting Kit-8 (CCK-8; #343-07623,
111 Dojindo) and calculated by setting that of DMSO-treated samples as 100%. KyPlot 5.0
112 software (KyensLab, Inc., Tokyo, Japan) was used to draw survival curves.[36] For growth
113 inhibition curves, the absorbance at the time of treatment (Tz) was measured 24 hours after
114 seeding, and the absorbance at the end of treatment (Ti) was measured 60 hours after
115 treatment. DMSO-treated cells were used as the control (C). Growth inhibition rates were
116 calculated as: $[(Ti-Tz)/(C-Tz)] \times 100$ for concentrations in which $Ti >/= Tz$, $[(Ti-Tz)/Tz] \times 100$
117 for concentrations in which $Ti < Tz$.[37]

118

119 **2.5 Apoptosis assay**

120 Apoptosis assay was performed using the FITC Annexin V Apoptosis Detection Kit I
121 (#556547, BD Biosciences, NJ, USA) according to the manufacturer's instructions. Briefly,
122 JuB4 and Re12 cells were treated with 10 μM SAHA or JQ1. One million cells were
123 suspended in the binding buffer and stained with annexin V. Cells were analyzed with a BD
124 FACSVerse flow cytometer (BD Biosciences, NJ, USA).

125

126 **2.6 RNA-Sequencing**

127 ISOS-1 were treated with 1 μM SAHA for 24 h, 1 μM JQ1 for 36 h, or 2 mM VPA
128 for 36 h in triplicate. Total RNA was extracted with a NucleoSpin RNA isolation kit
129 (#740955.50, Macherey-Nagel GmbH & Co. Düren, Germany) according to the
130 manufacturer's instructions. RNA samples were submitted to Kazusa DNA Research
131 Institution (Chiba, Japan) for further analyses. Sequencing reads were mapped to the mm39
132 mouse reference genome using STAR, and expression levels were estimated using RSEM.[38,39]
133 Differential expression and gene expression profiles were analyzed by edgeR and GSEA
134 v4.1.0, respectively.[40–42]

135

136 **2.7 SA-β-gal staining**

137 SA-β-gal staining was performed using a Senescence β-Galactosidase Staining Kit
138 (#9860, Cell Signaling Technology, MA, USA) according to the manufacturer's instructions.
139 Briefly, ISOS-1 was treated with DMSO or 10 μM JQ1 for 24 h and fixed with 4%
140 paraformaldehyde (PFA) for 10 min at RT. Cells were stained with β-Galactosidase Staining
141 Solution containing 5-bromo-4-chloro-3-indolyl β-D-galactopyranoside (X-Gal: #16495,
142 Cayman Chemical) for 13 h at 37°C. Positive cells were counted manually using an inverted
143 microscope (BIOREVO BZ-9000; KEYENCE, Tokyo, Japan).

144

145 **2.8 Cell cycle analysis**

146 ISOS-1, JuB2, JuB4, and Re12 cells were treated with DMSO or JQ1 for 24 hours.
147 ISOS-1 was treated with 10 μM JQ1, and other cell lines were treated with 5 μM JQ1. They

148 were stained with 30 μM bromodeoxyuridine (BrdU) for 45 min at 37°C, fixed in 70%
149 ethanol overnight and washed with 0.5% Triton X-100 in PBS (PBST). They were
150 resuspended in 500 μL of 2N HCl-0.5% Triton X-100 for 30 min at RT and neutralized with
151 500 μL of 0.1 M sodium borate buffer (pH 8.5) for 30 min at RT. Then, cells were blocked
152 with 1% bovine serum albumin (BSA, #017-23294, Wako) in PBST for 1 hour. 1.2×10^6 cells
153 were incubated with/without anti-BrdU monoclonal antibody (1:100; MOBU-1 clone,
154 #B35128, Thermo Fisher Scientific) in PBST with 1% BSA for 1 hour at RT and then stained
155 with donkey anti-mouse IgG (H+L) conjugated with AlexaFluor 488 (1:1,000; #A32766,
156 Thermo Fisher Scientific). DNA was stained with 25 μg/ml propidium iodide (PI, #P378,
157 Dojindo). Cell cycle and proliferation were analyzed with BD FACSVerse flow cytometer.
158 Results were analyzed with FCS Express version 4.

159

160 **2.9 Migration assay**

161 JuB4 and Re12 were treated with DMSO, 2 μM SAHA, or 2 mM VPA for 48 h in 6-
162 well plates. Then, after replacing the medium to the one without inhibitors, the cells were co-
163 cultured with RAW264 seeded on ThinCert Cell Culture Inserts (#657630, Greiner Bio-One)
164 for 24 h. RAW264 on the culture surface of the inserts were removed with a cotton swab.
165 Migrated RAW264 on the bottom side of the inserts were fixed with 4% PFA for 30 min at
166 RT and then stained with 0.01% crystal violet for 30 min at RT. The number of cells was
167 counted manually in 10 fields at 200× under a light microscope (BH-2; Olympus, Tokyo,
168 Japan).

169

170 **2.10 Western blotting**

171 SDS lysis buffer {2% SDS, 50 mM Tris-HCl (pH6.8), 1 mM EDTA (pH 8.0)} was
172 added to cultured cells or minced tumor tissues after washing them with PBS twice. Cell
173 lysates and the supernatant of the minced tumor tissues were then sonicated using BRANSON
174 Sonifier 450 (Branson Ultrasonics Corporation, CT, USA) for 2 seconds at power 2. 2 μg
175 protein was used for analysis. Primary antibody and secondary antibody reactions were done
176 in Can Get Signal Solution 1 (#NKB-101, TOYOBO, Osaka, Japan) overnight at 4°C in Can
177 Get Signal Solution 2 (TOYOBO) for 1 h at RT. Data were processed using ImageJ.[43]
178 Antibodies used in this study are listed in Table S2.

179

180 **2.11 Reverse transcription quantitative polymerase chain reaction (RT-qPCR)**

181 Total RNA was extracted with TriPure Isolation Reagent (#11667157001, Roche,
182 Basel, Switzerland). Reverse transcription was performed using Primescript II 1st strand
183 cDNA Synthesis Kit (#6210, Takara Bio, Kusatsu, Japan) for 1 μg total RNA of samples.
184 qPCR was performed using KAPA SYBR FAST qPCR Kit Master Mix (2×) ABI Prism
185 (KK4605, KAPA Biosystems, MA, USA). Primers are listed in Table S3. Results were
186 normalized using the geometric mean of reference genes (*RPL32* and *HPRT* for canine genes,
187 and *Hprt* and *Tbp* for murine genes), which were selected from potential internal controls by
188 geNorm (Fig. S1).[44] Primer efficiencies were between 90% and 110% for all primer sets (Fig.
189 S2). Relative expression levels were calculated by setting the expression levels in the DMSO-
190 treated samples as 1.

191

192 **2.12 Animal studies**

193 All mouse experiments were performed under the guidelines of an institute, which

194 follows the ARRIVE guidelines. Five-week-old female Balb/c and KSN/Slc mice (Japan
195 SLC, Inc. Shizuoka, Japan) were used. A day before tumor cell inoculation, KSN/Slc mice
196 were treated with 100 μL 2.5 mg/ml anti-asialo GM1 (#014-09801, Fujifilm Wako) to
197 increase the success rate of JuB2 transplantation.[45] Five million cells were inoculated
198 subcutaneously in both flanks of Balb/c and KSN/Slc mice. Tumor volumes were calculated
199 using the formula: Volume = (Length × $Width^2$)/2. When the tumor volume reached 100 mm^3,
200 inhibitor treatment was started. Mice were intraperitoneally injected with SAHA (150 mg/kg)
201 daily,[46] VPA (200 mg/kg) five times weekly,[47] or JQ1 (50 mg/kg) daily.[48,49] For preliminary
202 experiments, tumor tissues were collected from three mice for each inhibitor three days after
203 starting treatments and were subject to western blotting or IHC. Comparison in IHC was done
204 among the samples placed on the same slides. For treatment experiments, Balb/c mice were
205 euthanized with CO_2 when tumors reached 1,000 mm^3 in volume. KSN/Slc mice were
206 euthanized with CO_2 11 or 12 days after treatment initiation. Survival times were defined as
207 the period from beginning of drug administration to euthanasia.

208

209 **2.13 Statistical analysis**

210 Statistical analyses were performed with R (version 4.1.0). Fisher's exact test was
211 used to analyze the ratio of acetylated H3 staining levels. Student's *t*-test or Mann-Whitney
212 test were used to analyze the differences between two groups, whereas Tukey's test was used
213 to analyze differences among multiple groups. Survival curves were analyzed using the log-
214 rank test. Overall tumor growth was analyzed with two-way ANOVA.

215

216 **3. Results**

217 **3.1 Histone acetylation levels in HSA cells are high *in vitro* and heterogeneous *in vivo***

218 We first analyzed histone acetylation levels in HSA cell lines and CnAOEC. We
219 found that global acetylation of H2B, H3, and H4 was highly enriched in all HSA cell lines
220 compared with CnAOEC (Fig. 1A). Then, we examined global acetylated histone H3 levels in
221 10 clinical HSA cases. These cases were classified into three types according to their
222 histological pattern: solid, capillary, or cavernous.[1] Five cases had a single histological
223 pattern, while the other five possessed multiple proliferation patterns (Fig, 1B). We also
224 classified histone H3 acetylation levels into three groups based on the normalized values:
225 negative (< 0.5), weak (0.5–2.0), and strong (> 2.0) (Figs. 1C and 1D). The results showed
226 that the histone H3 acetylation levels of tumor cells were heterogeneous, and the ratio was
227 different depending on their histological pattern even in the same tumor tissue (Figs. 1E and
228 1F). Furthermore, the ratio of tumor cells classified as negative was the highest in the solid
229 pattern followed by the capillary pattern, and the lowest in the cavernous pattern (Fig. 1F).
230 These results suggest that histone H3 acetylation levels are heterogeneous in tumor cells and
231 are associated with their histopathological patterns.

232

233 **3.2 SAHA and JQ1 induce apoptosis in HSA cell lines**

234 To examine the roles of histone acetylation in HSA, we modified histone acetylation
235 levels using HDACi (SAHA and VPA) and BETi (JQ1) in canine and murine HSA cell lines.
236 First, we evaluated whether global histone acetylation levels were altered by these inhibitors.
237 SAHA and VPA treatments increased global histone acetylation levels in both canine and
238 murine HSA cell lines, whereas JQ1 decreased them in H2B, H3 and H4 of JuB2 and JuB4, in
239 H4 of Re21 and in H2B of ISOS-1 (Fig. 2A). Then, we examined the effects of HDACi and
240 BETi on HSA cell proliferation. SAHA and JQ1 treatment highly decreased the number of
241 cells, while VPA treatment did not affect their proliferation (Figs. 2B and S3A). IC_{50} values

242 of SAHA and JQ1 in HSA cell lines were almost or less than one-tenth of those in CnAOEC,
243 which indicated that HSA cell lines were more susceptible to these inhibitors than CnAOEC
244 (Fig. 2C). Then, we checked apoptosis markers and found that SAHA and JQ1 increased
245 cleaved caspase 3 expression levels and annexin V positivity in HSA cell lines except for
246 JQ1-treated ISOS-1 (Figs. 2D–F). Neither change was observed in VPA treatment (Figs. 2D,
247 S3B and S3C). Finally, we evaluated protein expression and phosphorylation levels of cell
248 survival proteins AKT and ERK. Although the results were different among the cell lines,
249 either total or phosphorylated AKT or ERK levels were downregulated by SAHA and JQ1 but
250 not by VPA (Fig. S4). These results suggest that SAHA and JQ1 induced apoptosis in HSA
251 cell lines except for ISOS-1 treated with JQ1, and that VPA did not induce cell death in all
252 HSA cell lines.
253
254 **3.3 SAHA and VPA activate inflammatory responses in HSA cell lines**
255 We further investigated the mechanisms of the effects of the inhibitors in HSA cells.
256 GSEA results indicated that inflammatory-related gene expression was positively correlated
257 in SAHA and VPA treatment in ISOS-1 (Fig. 3A). Consistent with this, *Il6*, *Cxcl1*, *Ccl2*,
258 *Ccl7*, and *Oas1a* were upregulated more than two-fold following treatment with either SAHA
259 or VPA or both (Fig. 3B). We wanted to extrapolate these findings to canine HSA, but
260 *CXCL1* does not exist in the canine genome, *CCL2* expression was not detected, and *CCL7*
261 expression was not increased by SAHA and VPA treatments. However, *OAS1*, the orthologue
262 of murine *Oas1a*, and other inflammatory-related genes were upregulated more than two-fold
263 in canine HSA cell lines treated with SAHA and/or VPA (Fig. 3C). Inflammatory responses
264 in tumor cells can induce immune cell migration, leading to host immune responses to tumor
265 tissues. Therefore, to corroborate whether SAHA and VPA treatment in HSA cell lines can
266 attract immune cells, a macrophage migration assay was performed using RAW264, a mouse

267 macrophage-like cell line (Fig. 3D). RAW264 migrated when they were co-cultured with
268 SAHA-treated JuB4 or VPA-treated Re12 (Fig. 3E) but not in ISOS-1 (Fig. S5). These results
269 suggest that SAHA and VPA can induce inflammatory responses in canine HSA cell lines.
270 This could attract macrophages, although it depends on the combination of cell lines and
271 HDACi.
272
273 **3.4 JQ1 induces autophagy and impedes the cell cycle in HSA cell lines**
274 We also investigated the genome-wide gene expression changes in JQ1-treated ISOS-
275 1. GSEA showed that autophagy-related gene expression and cell cycle related-gene
276 expression were positively and negatively correlated, respectively (Figs 4A and 4B). These
277 expression changes were validated by RT-qPCR (Fig. 4C). LC3-II, an active autophagy
278 marker, was expressed at higher levels in all JQ1-treated HSA cell lines except for Re12
279 compared with DMSO controls (Fig. 4D). Moreover, cotreatment of JQ1 and bafilomycin A1,
280 an inhibitor of autophagosome-lysosome fusion, further enhanced LC3-II expression (Fig.
281 4D). These results indicated that JQ1 activated initiation of autophagy in HSA cell lines but
282 not inhibited autophagosome degradation.
283 Although JQ1 treatment in ISOS-1 deceased cell viability, it did not increase
284 apoptosis marker expressions (Figs. 2C-F). These results led us to speculate that JQ1 retarded
285 cell proliferation but not actively induced cell death. To clarify this speculation, we generated
286 growth inhibition curves through which we could evaluate whether the cells actively died or
287 slowed their proliferation speed by JQ1 in ISOS-1. The results showed that growth inhibition
288 rates were positive even when the cells were treated with 10 μM JQ1, which indicated that
289 JQ1 mainly led to cell cycle delay in ISOS-1 (Fig. 5A). Then, we further evaluated cell cycle
290 status under JQ1 treatment in ISOS-1 and canine HSA cell lines. BrdU and propidium iodide
291 (PI) staining revealed that proliferating cells (BrdU+ cells) were significantly decreased in

292 both murine and canine HSA cell lines by JQ1 (Fig. 5B). PI signals showed that the
293 percentage of dead cells was slightly increased by JQ1 in ISOS-1, but its extent was lower
294 than in canine HSA cell lines (Fig. 5C). We also examined cell senescence by performing SA-
295 β-gal staining in ISOS-1 cells. The results indicated that JQ1-treated ISOS-1 showed a
296 significantly higher number of positive cells than DMSO-treated cells (Fig. 5D).
297 These results suggest that autophagy activation and cell cycle downregulation are
298 induced by JQ1, and that cell cycle retardation and cell senescence are major effects of JQ1 in
299 ISOS-1.
300
301 **3.5 JQ1 suppresses HSA tumor growth *in vivo***
302 Finally, to evaluate the treatment effects of SAHA, VPA, and JQ1 *in vivo*, we treated
303 ISOS-1 tumor-bearing Balb/c mice with SAHA, VPA, or JQ1. Three days SAHA and VPA
304 treatment increased global acetylated H3 levels in tumor tissues (Fig. S6A). Quantitative IHC
305 analysis revealed that global acetylated histone H3 levels in tumor cells were slightly
306 increased in SAHA and VPA treatments, whereas they were decreased in JQ1 treatments
307 (Figs. S6B - S6D). VPA treatments altered staining patterns in the nuclei of tumor cells
308 compared with the DMSO control (Fig. S6C, insets). Long term treatment experiments
309 revealed that only JQ1 slowed tumor growth and extended median and mean survival times
310 by 6 days and 5.6 days, respectively (Fig. 6A and B). JQ1 treatment in JuB2 tumor-bearing
311 KSN/Slc mice also suppressed JuB2 tumor growth (Fig. 6C). These treatments did not cause
312 body weight loss in mice (Fig. S7). These results suggest that JQ1 has suppressive effects on
313 HSA tumor growth *in vivo*.
314
315 **4. Discussion**
316 HSA tumor cells in clinical cases showed various H3 acetylation levels even in the

317 same tumor tissue. Moreover, this heterogeneity differed depending on the histological
318 pattern. These results can be explained by the differentiation status of the tumor cells. Global
319 histone acetylation levels have been reported to be increased as cells differentiate.[50,51]
320 Furthermore, HSA tumor cells forming the solid pattern are considered to be
321 undifferentiated.[52] Given that the percentage of tumor cells classified as H3 acetylation-
322 negative was high in the solid pattern, they could be more undifferentiated than other tumor
323 cells. Further research is required to clarify whether global histone acetylation levels reflect
324 the differentiation status of HSA tumor cells.

325 We demonstrated that SAHA and VPA upregulated inflammatory-related genes and
326 attracted RAW264 cells in JuB4 or Re12 cells. *OAS1* and *OAS2*, genes upregulated by SAHA
327 and VPA in canine HSA cells, are interferon-stimulated genes (ISGs).[53] Increased ISGs result
328 in tumor regression by turning immunologically cold tumors hot, thereby attracting anti-tumor
329 immune cells into tumor tissues. [54,55] Several reports indicated that HDACi activated immune
330 responses and enhanced immune cell functions.[56–58] According to these findings, HSA cells
331 could also gain anti-tumor effects by HDACi treatment. However, other upregulated genes in
332 our study, *CXCL8* and *CXCL12*, have been reported to promote tumor progression by several
333 mechanisms such as inducing angiogenesis or polarizing macrophages to an M2 state.[59–61]
334 Furthermore, given that a recent report demonstrated that a large numbers of M2-polarized
335 macrophages exist in HSA tumor tissues and HSA cells could induce M2 polarization in
336 macrophages,[32] HDACi might promote HSA tumor progression by upregulating the
337 expression of tumor-promoting cytokines such as *CXCL8* and *CXCL12*. Further research is
338 required to understand the effects of HDACi on tumor immunity.

339 In our study, SAHA and VPA did not either suppress or promote tumor growth of
340 ISOS-1 in an immunocompetent mouse model. This is explained by several possibilities.
341 First, histone deacetylases functioning in ISOS-1, which can be targeted by HDACi, might

342 differ from *in vitro* to *in vivo* conditions. Thus, HDACi effects might differ depending on the
343 experimental conditions. Second, the plasma concentrations of the drugs might be decreased
344 too fast to induce anti-tumor effects. In our experiment, global histone H3 acetylation levels
345 were only slightly increased by SAHA and VPA, although we referred to previous reports to
346 determine the dose (Fig. S6).[46–49] SAHA has been noted for its fast reduction in plasma
347 concentration in *in vivo* models.[62] Third, the conditions we tested did not induce anti-tumor
348 immune responses. Co-treatment with other drugs such as doxorubicin or immune checkpoint
349 inhibitors would be beneficial for HSA treatment by stimulating immune responses.[63–66]
350 Further research is required to investigate whether SAHA and VPA can be used as alternative
351 therapeutics in HSA.

352 In our study, JQ1 induced apoptosis, autophagy initiation, and tumor growth
353 suppression in canine HSA cells. Apoptosis is probably related to tumor growth suppression,
354 but no clear answer about whether autophagy had anti- or pro-tumor effects was obtained
355 from our study. This is because autophagy has two opposite roles in tumor cells:
356 cytoprotective and cytotoxic.[67] In ovarian cancer and acute myeloid leukemia in humans,
357 JQ1-induced autophagy had a cytoprotective role and an autophagy inhibitor enhanced the
358 anti-tumor effect of JQ1. [68,69] Conversely, in human bladder cancer cell lines, the proliferation
359 suppression capacity of JQ1 was attenuated by autophagy inhibitors, which suggested that
360 JQ1-induced autophagy had a cytotoxic role.[23] Further experiments are needed to elucidate
361 which roles JQ1-induced autophagy has in HSA.

362 Although the autophagy effects induced by JQ1 were not clear in our study, JQ1
363 suppressed tumor growth in both canine and murine HSA cell lines *in vivo*. JQ1 treatment did
364 not alter global histone H3 acetylation levels in tumor tissues, but those in tumor cells were
365 moderately decreased (Fig. S5). Several reports indicated that JQ1 induced minor changes in
366 histone marks but inhibited BET proteins, reader proteins for histone acetylation.[70–74] To

367 further understand how JQ1 affects tumor growth *in vivo,* local histone acetylation levels must
368 be investigated by chromatin immunoprecipitation (ChIP) or by the cleavage under targets
369 and release using nuclease (CUT&RUN) technique using tumor tissues treated with JQ1.
370 Several reports revealed that JQ1 or other BETis had anti-tumor effects, and clinical trials
371 were conducted in lymphoma, prostate cancer, and solid tumors.[24,75] Moreover, oral BETis
372 molibresib and INCB054329 induced tumor suppression in clinical and *in vivo* studies.[76,77]
373 Although further research is required, our results suggest that BETis could be an alternative
374 therapeutic for canine HSA.

375 In conclusion, we demonstrated that BETis can be used for HSA treatment. Although
376 further research is required, our results suggest that dysregulation of histone acetylation is
377 likely to be involved in HSA malignancy.

378

379 **References**

380 1. Kim JH, Graef AJ, Dickerson EB, Modiano JF. Pathobiology of hemangiosarcoma in
381 dogs: Research advances and future perspectives. *Vet Sci* 2015;2(4):388–405.
382 2. Clifford CA, Mackin AJ, Henry CJ. Treatment of canine hemangiosarcoma: 2000 and
383 beyond. *J Vet Intern Med* 2000;14(5):479–485.
384 3. Shustef E, Kazlouskaya V, Prieto VG, Ivan D, Aung PP. Cutaneous angiosarcoma: A
385 current update. *J Clin Pathol* 2017;70(11):917–925.
386 4. Leduc C, Jenkins SM, Sukov WR, Rustin JG, Maleszewski JJ. Cardiac angiosarcoma:
387 histopathologic, immunohistochemical, and cytogenetic analysis of 10 cases. *Hum*
388 *Pathol* 2017;60:199–207.
389 5. Megquier K, Turner-Maier J, Swofford R, et al. Comparative genomics reveals shared
390 mutational landscape in canine hemangiosarcoma and human angiosarcoma. *Mol*
391 *Cancer Res* 2019;17(12):2410–2421.

392 6. Kaelin WG, McKnight SL. Influence of metabolism on epigenetics and disease. *Cell*
393 2013;153(1):56–69.
394 7. Virani S, Virani S, Colacino JA, Kim JH, Rozek LS. Cancer epigenetics: a brief
395 review. *ILAR J*;53(3–4):359–369.
396 8. Xu R, Li C, Liu X, Gao S. Insights into epigenetic patterns in mammalian early
397 embryos. *Protein Cell* 2021;12(1):7–28.
398 9. Josling GA, Selvarajah SA, Petter M, Duffy MF. The role of bromodomain proteins in
399 regulating gene expression. *Genes (Basel)* 2012;3(2):320–343.
400 10. Clayton AL, Hazzalin CA, Mahadevan LC. Enhanced histone acetylation and
401 transcription: A dynamic perspective. *Mol Cell* 2006;23(3):289–296.
402 11. Calcagno DQ, Wisnieski F, Da Silva Mota ER, et al. Role of histone acetylation in
403 gastric cancer: Implications of dietetic compounds and clinical perspectives.
404 *Epigenomics* 2019;11(3):349–362.
405 12. Liu KY, Wang LT, Hsu SH. Modification of epigenetic histone acetylation in
406 hepatocellular carcinoma. *Cancers (Basel)* 2018;10(1):8.
407 13. West AC, Johnstone RW. New and emerging HDAC inhibitors for cancer treatment. *J*
408 *Clin Invest* 2014;124(1):30–39.
409 14. Bechter O, Schöffski P. Make your best BET: The emerging role of BET inhibitor
410 treatment in malignant tumors. *Pharmacol Ther* 2020;208:107479.
411 15. Claerhout S, Lim JY, Choi W, et al. Gene expression signature analysis identifies
412 vorinostat as a candidate therapy for gastric cancer. *PLoS One* 2011;6(9):e24662.
413 16. Lee YJ, Won AJ, Lee J, et al. Molecular mechanism of SAHA on regulation of
414 autophagic cell death in tamoxifen-resistant MCF-7 breast cancer cells. *Int J Med Sci*
415 2012;9(10):881–893.
416 17. Uehara N, Kanematsu S, Miki H, Yoshizawa K, Tsubura A. Requirement of p38

417 MAPK for a cell-death pathway triggered by vorinostat in MDA-MB-231 human
418 breast cancer cells. *Cancer Lett* 2012;315(2):112–121.
419 18. Yagi Y, Fushida S, Harada S, et al. Effects of valproic acid on the cell cycle and
420 apoptosis through acetylation of histone and tubulin in a scirrhous gastric cancer cell
421 line. *J Exp Clin Cancer Res* 2010;29(1):149.
422 19. Gameiro SR, Malamas AS, Tsang KY, Ferrone S, Hodge JW. Inhibitors of histone
423 deacetylase 1 reverse the immune evasion phenotype to enhance T-cell mediated lysis
424 of prostate and breast carcinoma cells. *Oncotarget* 2016;7(7):7390–7402.
425 20. Kortenhorst MS, Wissing MD, Rodríguez R, et al. Analysis of the genomic response of
426 human prostate cancer cells to histone deacetylase inhibitors. *Epigenetics*
427 2013;8(9):907–920.
428 21. Xue K, Gu JJ, Zhang Q, et al. Vorinostat, a histone deacetylase (HDAC) inhibitor,
429 promotes cell cycle arrest and re-sensitizes rituximab- and chemo-resistant lymphoma
430 cells to chemotherapy agents. *J Cancer Res Clin Oncol* 2016;142(2):379–387.
431 22. Jostes S, Nettersheim D, Fellermeyer M, et al. The bromodomain inhibitor JQ1 triggers
432 growth arrest and apoptosis in testicular germ cell tumours in vitro and in vivo. *J Cell*
433 *Mol Med* 2017;21(7):1300–1314.
434 23. Li F, Yang C, Zhang HB, et al. BET inhibitor JQ1 suppresses cell proliferation via
435 inducing autophagy and activating LKB1/AMPK in bladder cancer cells. *Cancer Med*
436 2019;8(10):4792–4805.
437 24. Wen N, Guo B, Zheng H, et al. Bromodomain inhibitor jq1 induces cell cycle arrest
438 and apoptosis of glioma stem cells through the VEGF/PI3K/AKT signaling pathway.
439 *Int J Oncol* 2019;55(4):879–895.
440 25. Gulay KCM, Aoshima K, Shibata Y, et al. KDM2B promotes cell viability by
441 enhancing DNA damage response in canine hemangiosarcoma. *J Genet Genomics*

442 2021;48(7):618–630.
443 26. Galli F, Aguilera JV, Palermo B, Markovic SN, Nisticò P, Signore A. Relevance of
444 immune cell and tumor microenvironment imaging in the new era of immunotherapy. *J*
445 *Exp Clin Cancer Res* 2020;39:89.
446 27. Sun X, Fu X, Xu S, et al. OLR1 is a prognostic factor and correlated with immune
447 infiltration in breast cancer. *Int Immunopharmacol* 2021;101 :108275.
448 28. Xia L, Oyang L, Lin J, et al. The cancer metabolic reprogramming and immune
449 response. *Mol Cancer* 2021;20(1):1–21.
450 29. Salemme V, Centonze G, Cavallo F, Defilippi P, Conti L. The crosstalk between tumor
451 cells and the immune microenvironment in breast cancer: Implications for
452 immunotherapy. *Front Oncol* 2021;11:289.
453 30. Lian X, Yang K, Li R, et al. Immunometabolic rewiring in tumorigenesis and anti-
454 tumor immunotherapy. *Mol Cancer* 2022;21(1):1–17.
455 31. Ghahremani MF, Radaelli E, Haigh K, et al. Loss of autocrine endothelial-derived
456 VEGF significantly reduces hemangiosarcoma development in conditional p53-
457 deficient mice. *Cell Cycle* 2014;13(9):1502–1508.
458 32. Gulay KCM, Aoshima K, Maekawa N, et al. Hemangiosarcoma cells induce M2
459 polarization and PD-L1 expression in macrophages. *Sci Rep* 2022;12:2124.
460 33. Bankhead P, Loughrey MB, Fernández JA, et al. QuPath: Open source software for
461 digital pathology image analysis. *Sci Rep* 2017;7(1):16878.
462 34. Murai A, Asa SA, Kodama A, Hirata A, Yanai T, Sakai H. Constitutive
463 phosphorylation of the mTORC2/Akt/4E-BP1 pathway in newly derived canine
464 hemangiosarcoma cell lines. *BMC Vet Res* 2012;8:128.
465 35. Masuzawa M, Fujimura T, Tsubokawa M, et al. Establishment of a new murine-
466 phenotypic angiosarcoma cell line (ISOS-1). *J Dermatol Sci* 1998;16(2) :91–98.

467 36. Yoshioka K. KyPlot as a tool for graphical data analysis. In:Härdle W, Önz B, eds.
468 Compstat. Physica, Heidelberg 2002;37–46.
469 37. National institutes of health. NCI-60 screening methodology. 2021.
470 https://dtp.cancer.gov/discovery_development/nci-60/methodology.htm. Accessed Oct.
471 21. 2021.
472 38. Dobin A, Gingeras TR. Mapping RNA-seq reads with STAR. *Curr Protoc Bioinforma*
473 2015;51(1):11.14.1-11.14.19.
474 39. Li B, Dewey CN. RSEM: Accurate transcript quantification from RNA-Seq data with
475 or without a reference genome. *BMC Bioinformatics* 2011;12:323.
476 40. Robinson MD, McCarthy DJ, Smyth GK. edgeR: A Bioconductor package for
477 differential expression analysis of digital gene expression data. 2009;26(1):139–140.
478 41. Mootha VK, Lindgren CM, Eriksson KF, et al. PGC-1α-responsive genes involved in
479 oxidative phosphorylation are coordinately downregulated in human diabetes. *Nat*
480 *Genet* 2003;34(3):267–273.
481 42. Subramanian A, Tamayo P, Mootha VK, et al. Gene set enrichment analysis: A
482 knowledge-based approach for interpreting genome-wide expression profiles. *Proc*
483 *Natl Acad Sci U S A* 2005;102(43):15545–15550.
484 43. Schneider CA, Rasband WS, Eliceiri KW. NIH image to ImageJ: 25 years of image
485 analysis. *Nat Methods* 2012;9(7):671–675.
486 44. Vandesompele J, De Preter K, Pattyn F, et al. Accurate normalization of real-time
487 quantitative RT-PCR data by geometric averaging of multiple internal control genes.
488 *Genome Biol* 2002;3(7):research0034.1–0034.11.
489 45. Yoshino H, Ueda T, Kawahata M, et al. Natural killer cell depletion by anti-asialo
490 GM1 antiserum treatment enhances human hematopoietic stem cell engraftment in
491 NOD/Shi-scid mice. *Bone Marrow Transplant* 2000;26(11):1211–1216.

492 46. Eto S, Saeki K, Yoshitake R, et al. Anti-tumor effects of the histone deacetylase
493 inhibitor vorinostat on canine urothelial carcinoma cells. *PLoS One*
494 2019;14(6):e0218382.
495 47. Terranova-Barberio M, Roca MS, Zotti AI, et al. Valproic acid potentiates the
496 anticancer activity of capecitabine in vitro and in vivo in breast cancer models via
497 induction of thymidine phosphorylase expression. *Oncotarget* 2016;7(7):7715.
498 48. Qiu H, Jackson AL, Kilgore JE, et al. JQ1 suppresses tumor growth through
499 downregulating LDHA in ovarian cancer. *Oncotarget* 2015;6(9):6915–6930.
500 49. Zhu X, Enomoto K, Zhao L, et al. Bromodomain and extraterminal protein inhibitor
501 JQ1 suppresses thyroid tumor growth in a mouse model. *Clin Cancer Res*
502 2017;23(2):430–440.
503 50. Ashktorab H, Belgrave K, Hosseinkhah F, et al. Global histone H4 acetylation and
504 HDAC2 expression in colon adenoma and carcinoma. *Dig Dis Sci* 2009;54(10):2109–
505 2117.
506 51. Golob JL, Paige SL, Muskheli V, Pabon L, Murry CE. Chromatin remodeling during
507 mouse and human embryonic stem cell differentiation. *Dev Dyn* 2008;237(5):1389–
508 1398.
509 52. Göritz M, Müller K, Krastel D, et al. Canine splenic haemangiosarcoma: Influence of
510 metastases, chemotherapy and growth pattern on post-splenectomy survival and
511 expression of angiogenic factors. *J Comp Pathol* 2013;149(1):30–39.
512 53. Justesen J, Hartmann R, Kjeldgaard NO. Gene structure and function of the 2'-5'-
513 oligoadenylate synthetase family. *Cell Mol Life Sci* 2000;57(11):1593–1612.
514 54. Sheng W, LaFleur MW, Nguyen TH, et al. LSD1 ablation stimulates anti-tumor
515 immunity and enables checkpoint blockade. *Cell* 2018;174(3):549-563.e19.
516 55. Zhang SM, Cai WL, Liu X, et al. KDM5B promotes immune evasion by recruiting

517 SETDB1 to silence retroelements. *Nature* 2021;598(7882):682–687.
518 56. Cox DJ, Coleman AM, Gogan KM, et al. Inhibiting histone deacetylases in human
519 macrophages promotes glycolysis, IL-1β, and T helper cell responses to
520 mycobacterium tuberculosis. *Front Immunol* 2020;11:1609.
521 57. Laengle J, Kabiljo J, Hunter L, et al. Histone deacetylase inhibitors valproic acid and
522 vorinostat enhance trastuzumab-mediated antibody-dependent cell-mediated
523 phagocytosis. *J Immunother Cancer* 2020;8(1):e000195.
524 58. Sun T, Li Y, Yang W, et al. Histone deacetylase inhibition up-regulates MHC class I to
525 facilitate cytotoxic T lymphocyte-mediated tumor cell killing in glioma cells. *J Cancer*
526 2019;10(23):5638–5645.
527 59. Xiong X, Liao X, Qiu S, et al. CXCL8 in tumor biology and its implications for clinical
528 translation. *Front Mol Biosci* 2022;9:235.
529 60. Guo F, Wang Y, Liu J, Mok SC, Xue F, Zhang W. CXCL12/CXCR4: A symbiotic
530 bridge linking cancer cells and their stromal neighbors in oncogenic communication
531 networks. *Oncogene* 2016;35(7):816–826.
532 61. Babazadeh S, Nassiri SM, Siavashi V, Sahlabadi M, Hajinasrollah M, Zamani-
533 Ahmadmahmudi M. Macrophage polarization by MSC-derived CXCL12 determines
534 tumor growth. *Cell Mol Biol Lett* 2021;26(1):1–15.
535 62. Fournel M, Bonfils C, Hou Y, et al. MGCD0103, a novel isotype-selective histone
536 deacetylase inhibitor, has broad spectrum antitumor activity in vitro and in vivo. *Mol*
537 *Cancer Ther* 2008;7(4):759–768.
538 63. Le DT, Durham JN, Smith KN, et al. Mismatch repair deficiency predicts response of
539 solid tumors to PD-1 blockade. *Science* 2017;357(6349):409–413.
540 64. Tubbs A, Nussenzweig A. Endogenous DNA damage as a source of genomic
541 instability in cancer. *Cell*;168(4):644–656.

542 65. Igase M, Nemoto Y, Itamoto K, et al. A pilot clinical study of the therapeutic antibody
543 against canine PD-1 for advanced spontaneous cancers in dogs. *Sci Rep*
544 2020;10(1):18311.
545 66. Maekawa N, Konnai S, Takagi S, et al. A canine chimeric monoclonal antibody
546 targeting PD-L1 and its clinical efficacy in canine oral malignant melanoma or
547 undifferentiated sarcoma. *Sci Rep* 2017;7(1):8951.
548 67. Gewirtz DA. The four faces of autophagy: Implications for cancer therapy. *Cancer Res*
549 2014;74(3):647–651.
550 68. Luan W, Pang Y, Li R, et al. Akt/mTOR-mediated autophagy confers resistance to bet
551 inhibitor JQ1 in ovarian cancer. *Onco Targets Ther* 2019;12:8063–8074.
552 69. Jang JE, Eom JI, Jeung HK, et al. AMPK-ULK1-mediated autophagy confers
553 resistance to BET inhibitor JQ1 in acute myeloid leukemia stem cells. *Clin Cancer Res*
554 2017;23(11):2781–2794.
555 70. Rathert P, Roth M, Neumann T, et al. Transcriptional plasticity promotes primary and
556 acquired resistance to BET inhibition. *Nature* 2015;525(7570):543–547.
557 71. Shu S, Lin CY, He HH, et al. Response and resistance to BET bromodomain inhibitors
558 in triple-negative breast cancer. *Nature* 2016;529(7586):413–417.
559 72. Kanno T, Kanno Y, Leroy G, et al. BRD4 assists elongation of both coding and
560 enhancer RNAs by interacting with acetylated histones. *Nat Struct Mol Biol*
561 2014;21(12):1047–1057.
562 73. Najafova Z, Tirado-Magallanes R, Subramaniam M, et al. BRD4 localization to
563 lineage-specific enhancers is associated with a distinct transcription factor repertoire.
564 *Nucleic Acids Res* 2017;45(1):127–141.
565 74. Kedaigle AJ, Reidling JC, Lim RG, et al. Treatment with JQ1, a BET bromodomain
566 inhibitor, is selectively detrimental to R6/2 Huntington's disease mice. *Hum Mol Genet*

567 2020;29(2):202–215.
568 75. Shorstova T, Foulkes WD, Witcher M. Achieving clinical success with BET inhibitors
569 as anti-cancer agents. *Br J Cancer* 2021;124(9):1478–1490.
570 76. Cousin S, Blay JY, Garcia IB, et al. Safety, pharmacokinetic, pharmacodynamic and
571 clinical activity of molibresib for the treatment of nuclear protein of the testis
572 carcinoma and other cancers: Results of a Phase I/II open-label, dose escalation study.
573 *Int J Cancer* 2022;150(6):993–1006.
574 77. Stubbs MC, Burn TC, Sparks R, et al. The novel bromodomain and extraterminal
575 domain inhibitor INCB054329 induces vulnerabilities in myeloma cells that inform
576 rational combination strategies. *Clin Cancer Res* 2019;25(1):300–311.
577

578 **Figure legends**

579 **Fig 1. Histone acetylation levels in HSA cells are high *in vitro* and heterogenous *in vivo.***
580 (A) Western blot analysis of acetylated histone H2B, H3, and H4. (B) Representative images
581 of HE and IHC staining in clinical HSA cases. Scale bars = 50 μm. (C) Box plots for
582 normalized nucleus DAB OD mean values in 10 clinical HSA cases. (D) Representative IHC
583 images of the classifications according to normalized acetylated H3 intensities in each
584 histological pattern. Arrowheads indicate the nuclei of tumor cells. (E) Stacked bar graphs
585 indicating the ratio of each staining level in 10 clinical cases. (F) Stacked bar graphs
586 comparing the ratio of each staining level according to the histological patterns in all cases or
587 within each case. *$P < 0.05$, **$P < 0.01$. Fisher's exact test.
588

589 **Fig 2. SAHA and JQ1 induce apoptosis in HSA cell lines.**
590 (A) Western blot analysis of acetylated H2B, H3, and H4 in canine HSA cell lines (JuB2,
591 JuB4, Re12) and a murine HSA cell line (ISOS-1) treated with DMSO, SAHA, JQ1, or VPA.

592 (B) Phase contrast images of canine and murine HSA cell lines 48 h after treatment with
593 DMSO, SAHA, VPA, or JQ1. Scale bars = 100 μm. (C) Survival curves (top) and IC_{50} values
594 (bottom) of canine and murine HSA cell lines treated with SAHA or JQ1 for 60 h. All
595 samples were analyzed in triplicate. Data are plotted as average percentages ± SD. (D)
596 Western blot analysis of cleaved caspase 3 in canine and murine HSA cells treated with
597 DMSO, SAHA, VPA, or JQ1. (E) Annexin V staining of canine and murine HSA cells treated
598 with DMSO, SAHA, or JQ1. (F) Percentages of apoptotic cells (annexin V-positive) in canine
599 and murine HSA cells treated with DMSO, SAHA, or JQ1. All samples were analyzed in
600 triplicate. Data are plotted as average percentages ± SD. *$P < 0.05$, **$P < 0.01$. Tukey's test.
601
602 **Fig 3. SAHA and VPA activate inflammatory responses in HSA cell lines.**
603 (A) (Left) GSEA results in ISOS-1 treated with SAHA (top) or VPA (bottom). Inflammatory-
604 related gene sets are highlighted in red. The number of genes in each gene set is shown next
605 to each bar. (Right) Representative GSEA plots of enriched gene sets in ISOS-1 treated with
606 SAHA (top) or VPA (bottom). (B) RT-qPCR results of genes related to inflammatory
607 responses in ISOS-1 treated with SAHA or VPA. (C) RT-qPCR results of inflammatory-
608 related genes in JuB4 and Re12 treated with SAHA or VPA. (D) Graphical images of
609 migration assay. (E) Quantitative analysis of migrated RAW264 cells co-cultured with SAHA
610 or VPA-treated Re12. Data are plotted as average percentages ± SD. *$P < 0.05$, **$P < 0.01$.
611 Tukey's test.
612
613 **Fig 4. JQ1 treatment induces autophagy in canine and murine HSA cell lines.**
614 (A) Positively (top) or negatively (bottom) enriched gene sets by GSEA in ISOS-1 treated
615 with JQ1 compared with DMSO-treated cells. The number of genes in each gene set is shown
616 next to each bar. (B) Representative GSEA plots of positively (top) and negatively (bottom)

617 enriched gene sets. (C) RT-qPCR of genes related to autophagy (top) and cell cycle (bottom)
618 in ISOS-1 treated with DMSO or JQ1. (D) Western blot analysis for LC3 expression in
619 canine and murine HSA cell lines treated with DMSO, JQ1 (10 μM, 24 hours) and/or
620 bafilomycin A1(100 nM, 3 hours). Data are plotted as average percentages ± SD.
621
622 **Fig. 5. JQ1 treatment impedes the cell cycle in canine and murine HSA cell lines.**
623 (A) A growth inhibition curve of ISOS-1 treated with JQ1. All samples were analyzed in
624 triplicate. Data are plotted as average percentages ± SD. (B) Density plots (left) and
625 quantitative analysis (right) of BrdU-positive cells in canine and murine HSA cell lines
626 treated with DMSO or JQ1. All samples were analyzed in triplicate. (C) Histograms of PI-
627 positive cells (left) and quantitative analysis of dead cells (right) in canine and murine HSA
628 cell lines treated with DMSO and JQ1. All samples were analyzed in triplicate. (D) (Left)
629 Representative images of SA-β-gal staining in ISOS-1 treated with DMSO or JQ1.
630 Arrowheads indicate positive cells. (Right) Quantitative analysis of SA-β-gal-positive cells.
631 Positive cells were counted in 10 fields under 200× magnification with a light microscope.
632 The average numbers were plotted with ± SD. Scale bars = 100 μm. *$P < 0.05$, **$P < 0.01$.
633 Student's *t*-test.
634
635 **Fig 6. JQ1 suppresses HSA tumor growth *in vivo.***
636 (A) Kaplan–Meier survival curves of ISOS-1-inoculated Balb/c mice treated with DMSO
637 (n=5), SAHA (n=5), VPA (n=4), or JQ1 (n=5). Days were counted after initiating drug
638 treatment. *P*-values were calculated using the log-rank test. (B) Individual growth curves of
639 ISOS-1 tumors in Balb/c mice treated with DMSO, SAHA, VPA, or JQ1 after treatment
640 initiation. (C) (Left) Individual tumor growth curves of JuB2 tumors in KSN/Slc mice treated
641 with DMSO or JQ1. The day when the treatment began was defined as day 1. ***$P < 0.001$.

642 Two-way ANOVA. (Right) Box plots of relative tumor volumes on the last day in KSN/Slc

643 mice treated with DMSO or JQ1. Relative tumor volumes were calculated by dividing the

644 tumor volume on the last day by that at day 1. *$P < 0.05$, Mann-whitney U test.

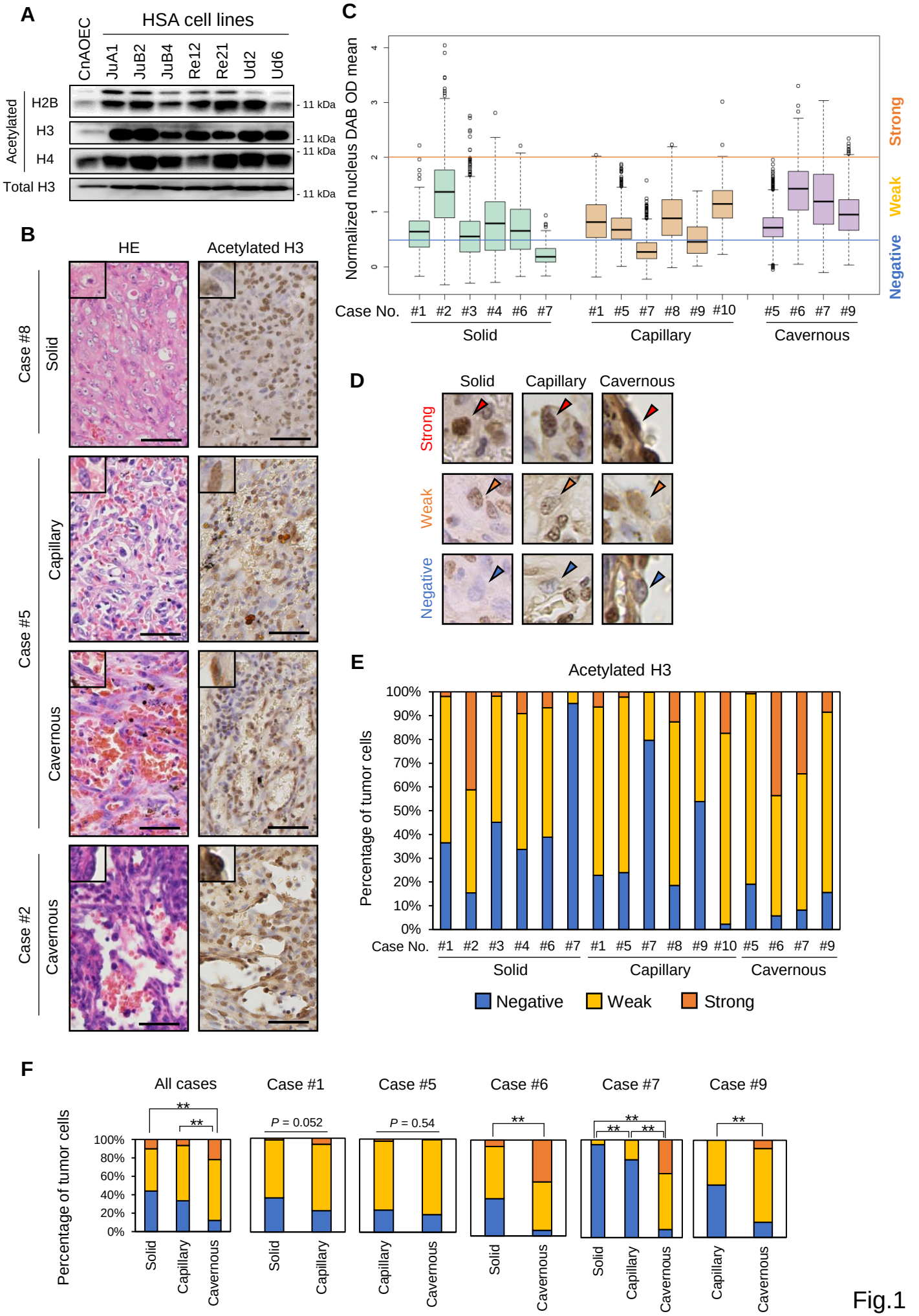
A
HSA cell lines
CnAOEC
JuA1
JuB2
JuB4
Re12
Re21
Ud2
Ud6
Acetylated
H2B
H3
H4
Total H3
11 kDa
B
HE
Acetylated H3
Case #8
Solid
Case #5
Capillary
Cavernous
Case #2
Cavernous
C
Normalized nucleus DAB OD mean
Strong
Weak
Negative
Case No.
#1 #2 #3 #4 #6 #7
#1 #5 #7 #8 #9 #10
#5 #6 #7 #9
Solid
Capillary
Cavernous
D
Solid
Capillary
Cavernous
Strong
Weak
Negative
E
Acetylated H3
Percentage of tumor cells
100%
90%
80%
70%
60%
50%
40%
30%
20%
10%
0%
Case No.
#1 #2 #3 #4 #6 #7
#1 #5 #7 #8 #9 #10
#5 #6 #7 #9
Solid
Capillary
Cavernous
Negative
Weak
Strong
F
All cases
Case #1
Case #5
Case #6
Case #7
Case #9
Percentage of tumor cells
100%
80%
60%
40%
20%
0%
**
P = 0.052
P = 0.54
Solid
Capillary
Cavernous

Fig.1

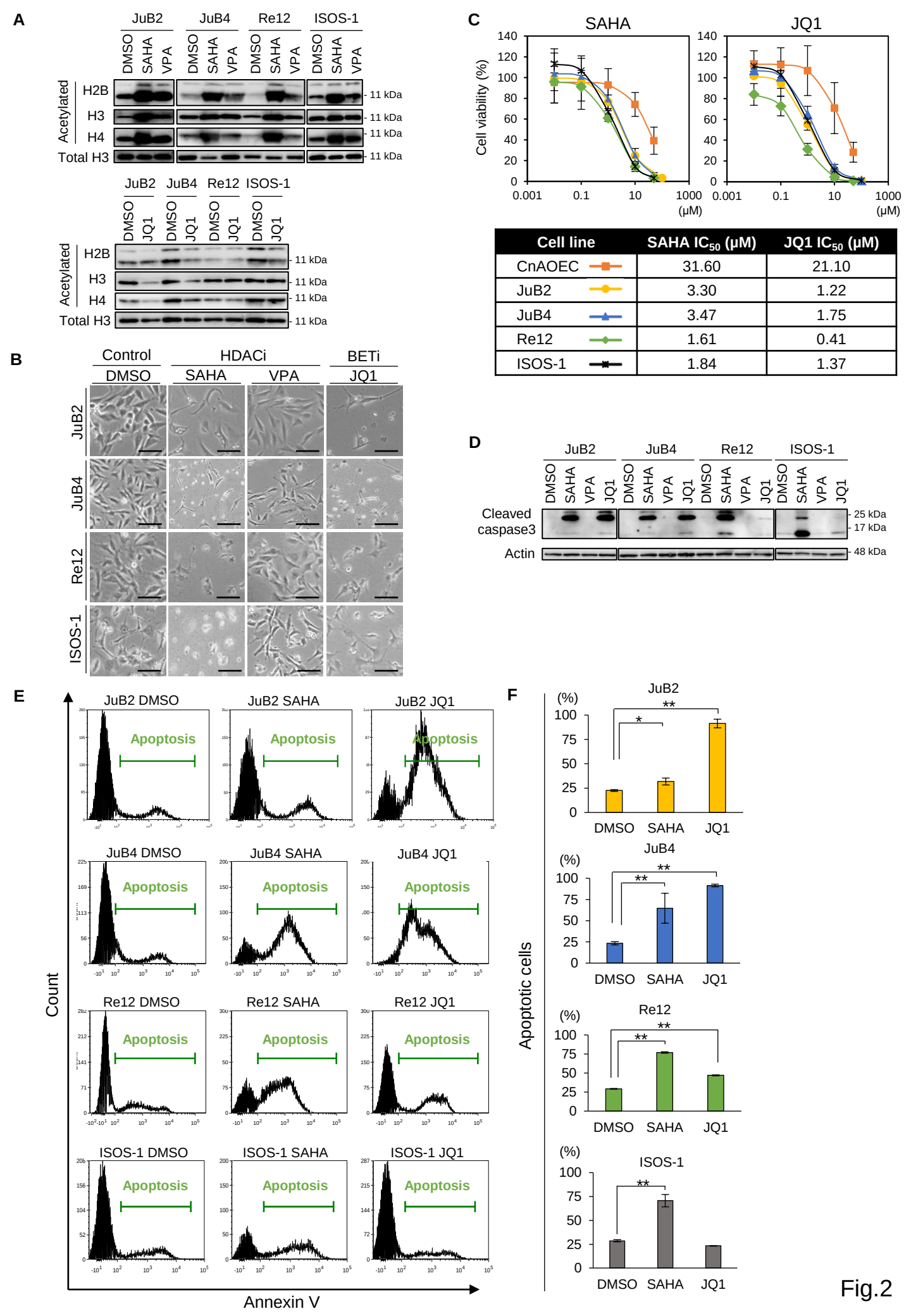

Cell line	SAHA IC_{50} (μM)	JQ1 IC_{50} (μM)
CnAOEC	31.60	21.10
JuB2	3.30	1.22
JuB4	3.47	1.75
Re12	1.61	0.41
ISOS-1	1.84	1.37

Fig.2

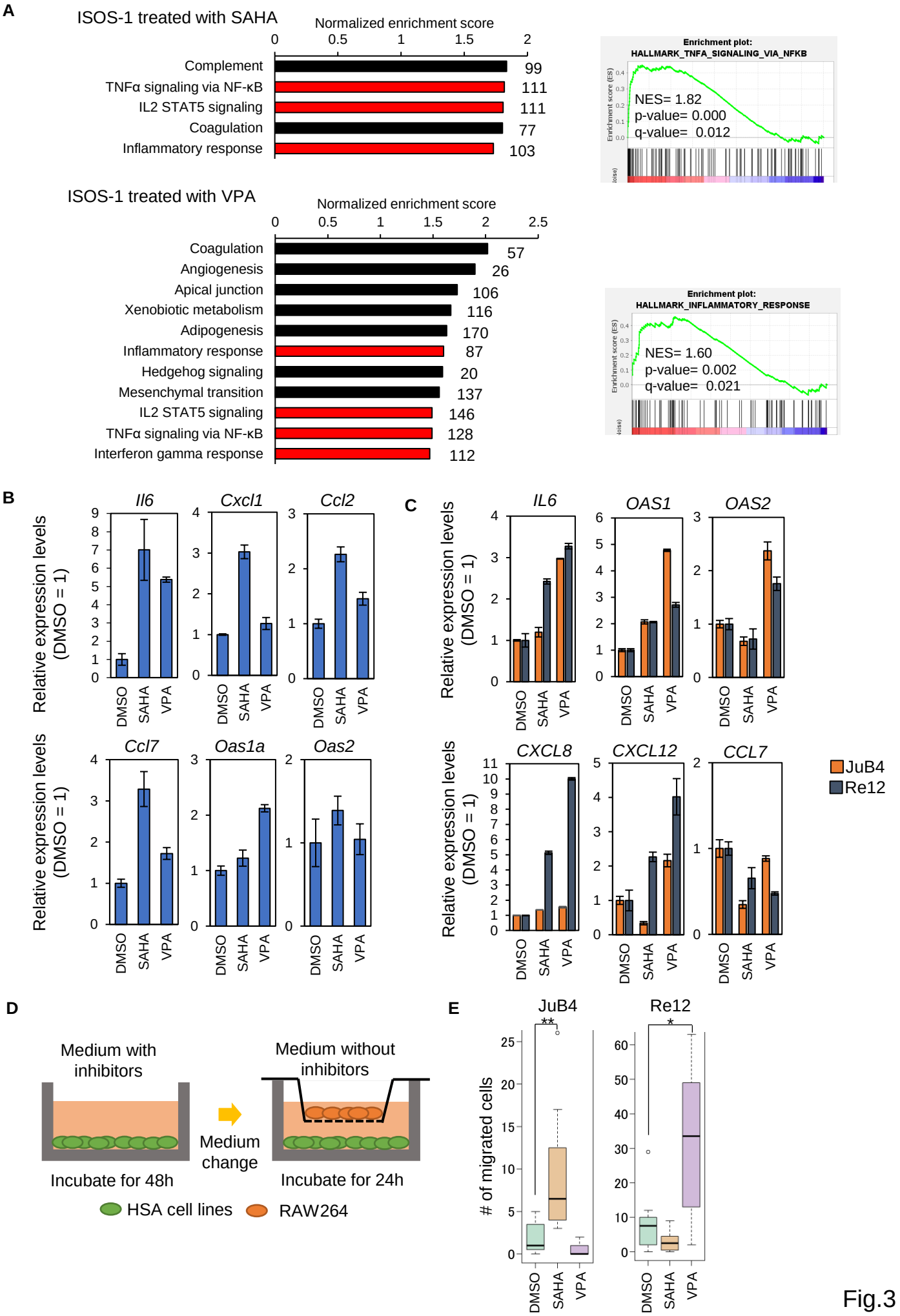
A
ISOS-1 treated with SAHA
Normalized enrichment score
0
0.5
1
1.5
2
Complement
TNFα signaling via NF-κB
IL2 STAT5 signaling
Coagulation
Inflammatory response
99
111
111
77
103
Enrichment plot:
HALLMARK_TNFA_SIGNALING_VIA_NFKB
NES= 1.82
p-value= 0.000
q-value= 0.012
ISOS-1 treated with VPA
Normalized enrichment score
0
0.5
1
1.5
2
2.5
Coagulation
Angiogenesis
Apical junction
Xenobiotic metabolism
Adipogenesis
Inflammatory response
Hedgehog signaling
Mesenchymal transition
IL2 STAT5 signaling
TNFα signaling via NF-κB
Interferon gamma response
57
26
106
116
170
87
20
137
146
128
112
Enrichment plot:
HALLMARK_INFLAMMATORY_RESPONSE
NES= 1.60
p-value= 0.002
q-value= 0.021
B
Il6
Cxcl1
Ccl2
Ccl7
Oas1a
Oas2
Relative expression levels
(DMSO = 1)
DMSO
SAHA
VPA
C
IL6
OAS1
OAS2
CXCL8
CXCL12
CCL7
JuB4
Re12
D
Medium with
inhibitors
Medium without
inhibitors
Medium
change
Incubate for 48h
Incubate for 24h
HSA cell lines
RAW264
E
JuB4
Re12
**
*
# of migrated cells
DMSO
SAHA
VPA

Fig.3

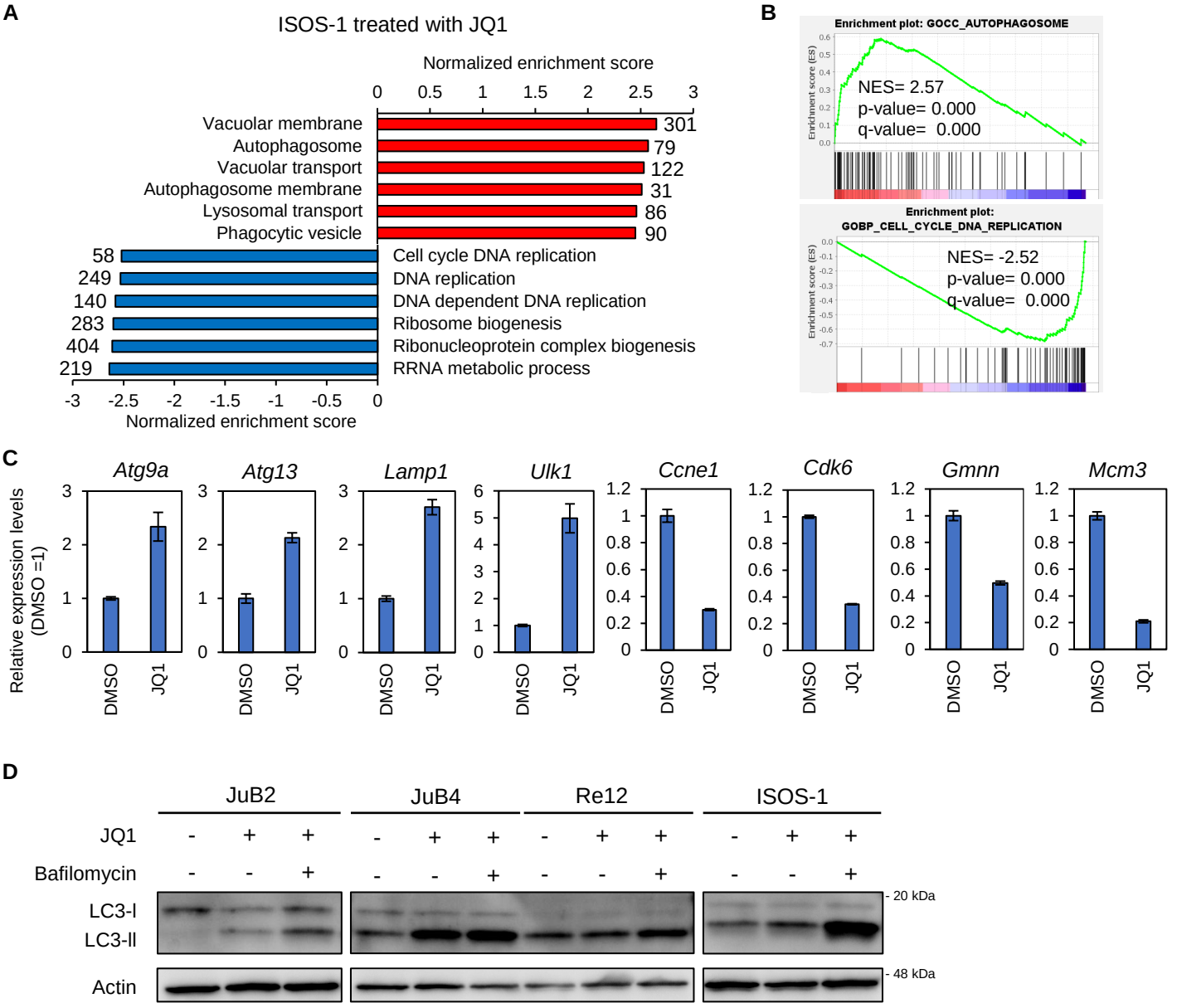
A
ISOS-1 treated with JQ1
Normalized enrichment score
0 0.5 1 1.5 2 2.5 3
Vacuolar membrane 301
Autophagosome 79
Vacuolar transport 122
Autophagosome membrane 31
Lysosomal transport 86
Phagocytic vesicle 90
58 Cell cycle DNA replication
249 DNA replication
140 DNA dependent DNA replication
283 Ribosome biogenesis
404 Ribonucleoprotein complex biogenesis
219 RRNA metabolic process
-3 -2.5 -2 -1.5 -1 -0.5 0
Normalized enrichment score
B
Enrichment plot: GOCC_AUTOPHAGOSOME
Enrichment score (ES)
NES= 2.57
p-value= 0.000
q-value= 0.000
Enrichment plot:
GOBP_CELL_CYCLE_DNA_REPLICATION
Enrichment score (ES)
NES= -2.52
p-value= 0.000
q-value= 0.000
C
Relative expression levels (DMSO =1)
Atg9a
Atg13
Lamp1
Ulk1
Ccne1
Cdk6
Gmnn
Mcm3
DMSO
JQ1
D
JuB2
JuB4
Re12
ISOS-1
JQ1 - + + - + + - + + - + +
Bafilomycin - - + - - + - - + - - +
LC3-I
LC3-II
Actin
20 kDa
48 kDa

Fig.4

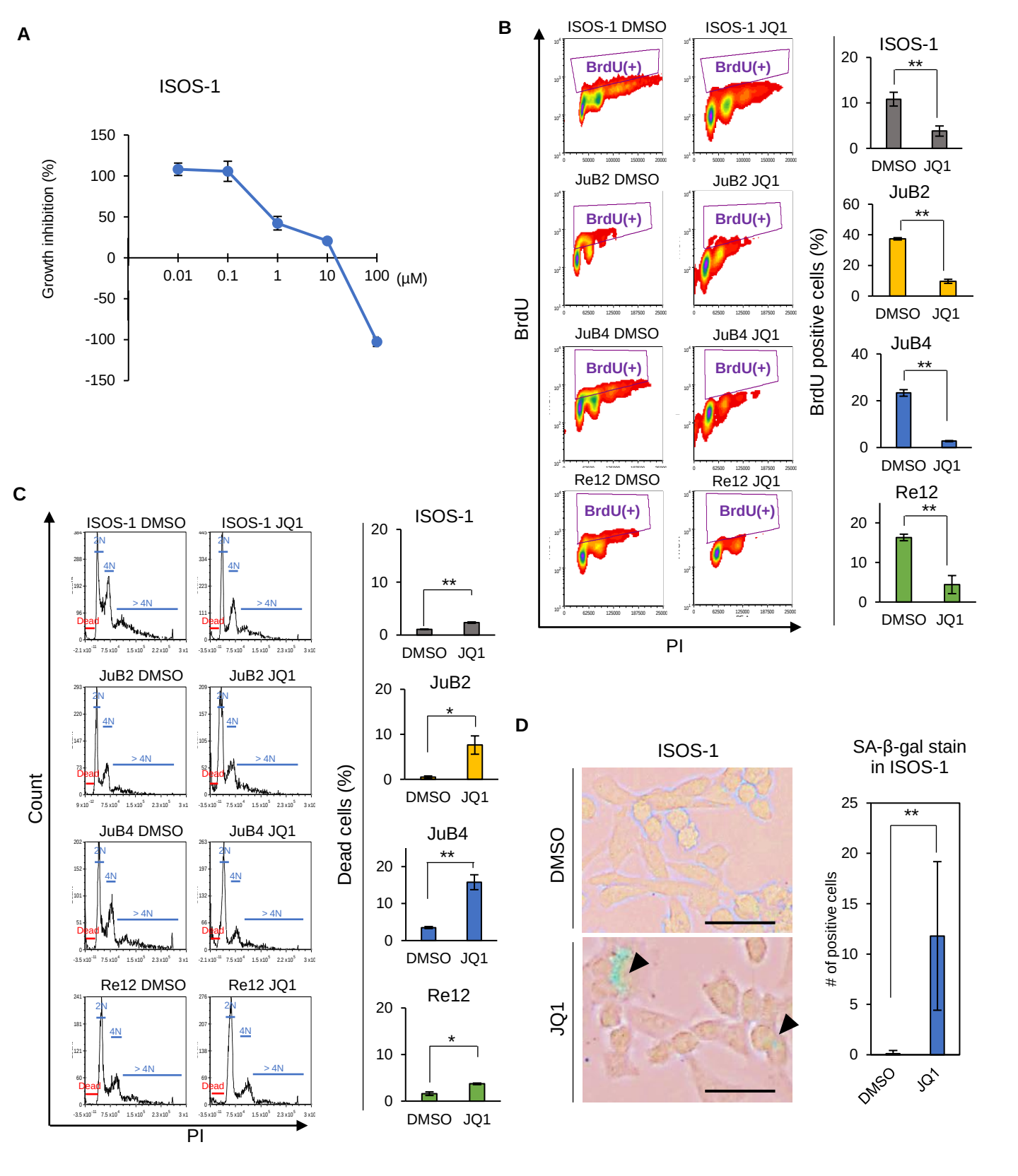
A
ISOS-1
Growth inhibition (%)
150
100
50
0
-50
-100
-150
0.01
0.1
1
10
100
(μM)
B
ISOS-1 DMSO
ISOS-1 JQ1
JuB2 DMSO
JuB2 JQ1
JuB4 DMSO
JuB4 JQ1
Re12 DMSO
Re12 JQ1
BrdU(+)
BrdU
PI
BrdU positive cells (%)
ISOS-1
JuB2
JuB4
Re12
DMSO
JQ1
**
C
ISOS-1 DMSO
ISOS-1 JQ1
JuB2 DMSO
JuB2 JQ1
JuB4 DMSO
JuB4 JQ1
Re12 DMSO
Re12 JQ1
2N
4N
> 4N
Dead
Count
PI
Dead cells (%)
ISOS-1
JuB2
JuB4
Re12
DMSO
JQ1
*
**
D
ISOS-1
DMSO
JQ1
SA-β-gal stain
in ISOS-1
# of positive cells
DMSO
JQ1
**

Fig.5

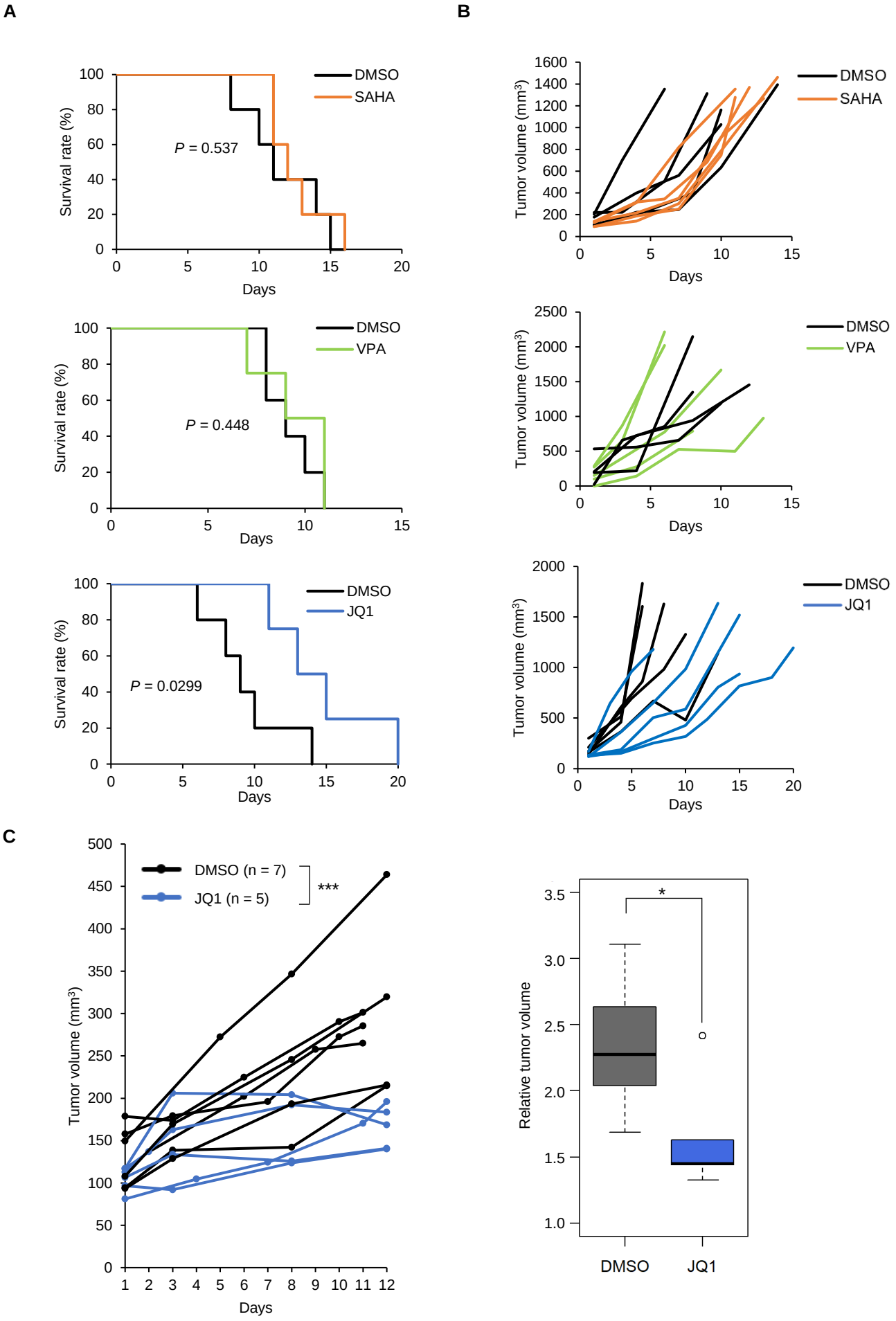
A
B
C
Survival rate (%)
Days
DMSO
SAHA
P = 0.537
VPA
P = 0.448
JQ1
P = 0.0299
Tumor volume (mm³)
DMSO (n = 7)
JQ1 (n = 5)
***
Relative tumor volume
*
DMSO
JQ1

Fig.6